A&A 487, 147–160 (2008)
DOI: 10.1051/0004-6361:200809706

Astronomy & Astrophysics

The fundamental plane of dwarf irregular galaxies⋆

O. Vaduvescu[1] and M. L. McCall[2]

[1] Instituto de Astronomía, Universidad Católica del Norte, Avenida Angamos 0610, Antofagasta, Chile
e-mail: ovidiu.vaduvescu@gmail.com
[2] York University, Department of Physics and Astronomy, 4700 Keele Street, M3J 1P3, Toronto, ON, Canada

Received 3 March 2008 / Accepted 19 May 2008

ABSTRACT

Aims. Near-IR photometry of dwarf irregular galaxies (dIs) has been acquired to expand the sample of objects suitable for investigating the fundamental plane (FP) discovered previously by us. Data for blue compact dwarfs (BCDs), dwarf ellipticals (dEs), and dwarf spheroidal galaxies (dSphs) are amalgamated to evaluate how closely these classes of galaxies are related to dIs.
Methods. Surface brightness profiles for dIs are modeled using a hyperbolic secant function (sech), which has been shown to sample the old galaxy component observed in the NIR (K_s). Also, profiles for BCDs are modeled using a sech function, but to this is added a Gaussian burst. Kinematics for dIs and BCDs are constrained by the width W_{20} of integrated HI line profiles, and motions within dEs and dSphs are judged from stellar velocity dispersions.
Results. The existence of a FP for dIs is confirmed. Omitting extreme deviants, the scatter of dIs about the plane is 0.43 mag, somewhat higher than expected from observational errors alone. Corrections of line widths for tilt do not reduce the residuals, so motions must be predominantly random. Corrections of surface brightnesses for tilt have no effect either. BCDs and dEs lie precisely on the FP defined by dIs, suggesting strong underlying connections among dIs, BCDs, and dEs.

Key words. galaxies: dwarf – galaxies: irregular – galaxies: photometry – galaxies: structure – infrared: galaxies – cosmology: distance scale

1. Introduction

Since the discovery of the Faber-Jackson relation for elliptical galaxies (Faber & Jackson 1976) and the Tully-Fisher relation for spiral galaxies (Tully & Fisher 1977), many authors have looked for inter-connections among the physical parameters of massive galaxies. Djorgovski & Davis (1987) were the first to recognize the so-called "fundamental plane" of elliptical galaxies, which links kinematics to length and brightness scales. During the last few years, fundamental planes have been identified for other massive entities such as spiral galaxies (Han et al. 2001), early type galaxies (Reda et al. 2005), radio galaxies (Bettoni et al. 2003), AGNs (Woo et al. 2004; Wang et al. 2006), quasars (Hamilton et al. 2006), and black holes (Kording et al. 2006; Merloni et al. 2003). Although Kormendy (1985) did a pioneering study of pair-wise correlations of parameters characterizing dwarfs, more sophisticated relationships have been elusive. What is clear is that the Tully-Fisher relation breaks down at low luminosities, probably because motions are no longer dominated by rotation.

Recently, deep imaging in the near-infrared and a breakthrough in the characterization of light profiles have led to the recognition of a fundamental plane (FP) for dwarf irregular galaxies (dIs). Vaduvescu et al. (2005 – V05 from now on) found that dI surface brightness profiles can be modeled using a sech function. They found a strong correlation among the sech absolute magnitude measured in K_s (M_{K_s}), the central surface brightness of the sech function (μ_{0K}), and the neutral hydrogen line width (W_{20}). Furthermore, Vaduvescu et al. (2006) discovered that light profiles for blue compact dwarf galaxies (BCDs) can be modeled as a Gaussian burst on top of a sech profile, making ready separation of young and old components possible. Thus, the FP for dIs provides an avenue to establish with greater clarity how closely BCDs (and other classes of dwarfs) may be related to dIs.

In this paper, we continue our study of the FP for dIs by expanding the sample of objects with good near-infrared photometry. We also make use of improved distances published recently in the literature. To complete the dwarf picture, we also address in the FP context two other classes of dwarf galaxies, namely BCDs and dwarf ellipticals (dEs).

In Sect. 2 we list criteria for selecting the sample of dwarfs presented in this paper. Our previous observations which defined the FP initially are reviewed in Sect. 3. Data from 2MASS of value to this study is discussed in Sect. 4. New observations acquired at CFHT and CTIO are presented in Sect. 5. Homogenized distances for our galaxies are derived in Sect. 6. The FP for dIs is examined in Sect. 7, and its relation to other dwarf classes is discussed in Sect. 8. In Sect. 9 we present conclusions.

2. The sample

To investigate the FP for dIs, good distances are required. Consequently, our sample of dIs is restricted to objects in the Local Volume. The Local Volume (LV) is defined to encompass all galaxies within about 10 Mpc on a scale where the

⋆ Based on observations acquired from CTIO, CFHT and 2MASS.

distance modulus of the LMC is 18.50 (Karachentsev et al. 2004). Cepheids (CEPH) and/or the tip of the red giant branch (TRGB) have been detected for many dIs in the LV, making possible the determination of accurate distances. For a few objects lacking such data, though, the Hubble law (HUB) or the three brightest stars (3BS) are employed to derive distances.

Further guiding the selection of dIs was size. To maximize observing efficiency, we emphasized targets which would fit into one quarter of the field of NIR detectors available at CFHT or CTIO. This made it possible to measure the sky background without moving the target off the infrared array. Data for the largest objects were extracted from 2MASS.

In this paper, we enlarge the sample of 19 dIs presented in V05 by 25. Of those, 8 objects were observed by 2MASS, 8 were observed at CFHT, and 9 were observed at CTIO.

3. Published data

In a previous paper (V05), we conducted an extensive examination of the surface brightness profiles of dIs in the NIR in an effort to identify a unifying mathematical description. Many functions were assessed, including exponential, de Vaucouleurs, and Sersic profiles, as well as "mixed" and "truncated" profiles. We concluded that a simple hyperbolic secant function (sech) fits the surface brightness profiles of the majority of dIs to a high degree of accuracy (mostly within 0.1 mag). According to this law, the fitted flux I at the distance r from the centre along the semi-major axis can be expressed as a function of only two parameters, namely the central surface brightness, I_0, and scale length, r_0:

$$I = I_0 \mathrm{sech}(r/r_0) = \frac{I_0}{\cosh(r/r_0)} = \frac{2I_0}{e^{r/r_0} + e^{-r/r_0}} \cdot \quad (1)$$

We define the "apparent sech magnitude" m_{SK} to be the integral of the surface brightness model out to a infinite radius. Because detection thresholds vary, this measure of brightness provides a more homogeneous descriptor of total flux than the apparent isophotal magnitude m_{TK}, which is derived from the total flux within the faintest detectable isophote. Furthermore, V05 have shown that it is a good approximation to the brightness of the old population, which is what is most relevant to structural studies.

Values of r_0, I_0, m_{SK}, and m_{TK} for our original sample are provided in V05. For the 2MASS, CFHT, and CTIO samples presented here, they are given in Table 2.

4. 2MASS data

Between 1997 and 2001, the Two Micron All Sky Survey (2MASS) imaged virtually the entire sky in the NIR (J, H, and K_s). The survey was taken using relatively small exposures (7.8 s co-added), employing two 1.3 m telescopes located at Mount Hopkins Observatory in Arizona and CTIO in Chile (Skrutskie 2006). Although most dwarfs failed to be imaged by 2MASS due to their faint surface brightness, a few bright dIs were detected. We searched the 2MASS Atlas in order to extract all field dwarfs imaged with a S/N at K_s sufficiently good to make possible solid fits to the light profiles. Eight dIs were selected for this paper. For the calibration, we employed the zero points included in the original image headers.

Following the approach in V05, we removed first all resolved sources from the original 2MASS image. Usually, these include Galactic stars in the foreground, young stars resolved in the host dwarf, and some extragalactic sources in the background. To remove all these sources, we used KILLALL, an IRAF script built around the DAOPHOT package (Buta & McCall 1999). The output is a "cleaned" image showing only the old unresolved component of the galaxy and a resolved sources catalog. Surface photometry was performed on the cleaned image using the task ELLIPSE in STSDAS. Then a sech law was fitted to the unresolved component (using the task NFIT1D).

Each of the dIs studied is displayed in Fig. 1. Panels on the left show the original 2MASS K_s images, while the right panels display the surface photometry and the sech fits. Fitting parameters and magnitudes are given in the first section of Table 2.

5. Observations

It is difficult to observe faint extended sources in the NIR due to the fact that the sky is very bright and variable in a short time-frame. An additional problem is that the background due to the detector and thermal radiation may vary both temporally and spatially (Vaduvescu & McCall 2004). Given these factors, we adopted a prudent strategy of observing the sky for as long a time as the targets, shifting between target and sky at a rate fast enough to resolve temporal variations in the background. This approach allowed us to observe dwarfs as deep as 24 mag arcsec^{-2} in K_s, consistent with our previous work. We present a log of our observations in Table 1.

5.1. CFHT observations

On Mar. 5–8, 2004 we acquired NIR imaging at the $f/8$ Cassegrain focus of the 3.6 m Canada-France-Hawaii Telescope (CFHT) located atop Mauna Kea, Hawaii (Run ID: 2004-AC23). Due to a technical problem at CFHT, one additional night (Feb. 23/24, 2004) was allocated to the same proposal, being observed by the CFHT staff in service mode. From four nights of the run, data were acquired during three, one being clouded out (Mar. 5/6, 2007). During the last two clear nights, humidity was variable and going high at times. The Moon was within five days of full.

We employed the CFHT-IR camera equipped with a HgCdTe array with 1024 × 1024 pixels and the K_s filter. The scale was $0\farcs211$ pix^{-1}, yielding a $3\farcm6 \times 3\farcm6$ FOV. Data were reduced in the manner described by V05, with calibrations being determined using 2MASS stars in the fields of view of the targets (typically 5, but as low as 1 or 2 for UGC 5764 and UGC 7408). Surface brightness profiles and fits to them were derived as described above for the 2MASS data.

Imaging and photometry of eight targets are presented here. Another three galaxies (UGC 4483, UGC 5423, and Sextans A) were presented in V05. In the left panels of Fig. 2, we show the reduced CFHT images, while in the right panels we display the surface photometry and the sech fits. In the second section of Table 2, we list the fitting parameters and magnitudes.

5.2. CTIO observations

On Aug. 1–3, 2007, we acquired NIR imaging using the 4 m Blanco telescope located at Cerro Tololo Interamerican Observatory, Chile (Run ID: 2007B-0907). We employed the ISPI camera equipped with a Hawaii array with 2048×2048 pixels mounted at the $f/8$ Cassegrain focus. The scale was $0\farcs3$ pix^{-1}, yielding a $10\farcm25 \times 10\farcm25$ FOV. For all targets, we used only the K_s filter. The first night was clouded out, while the

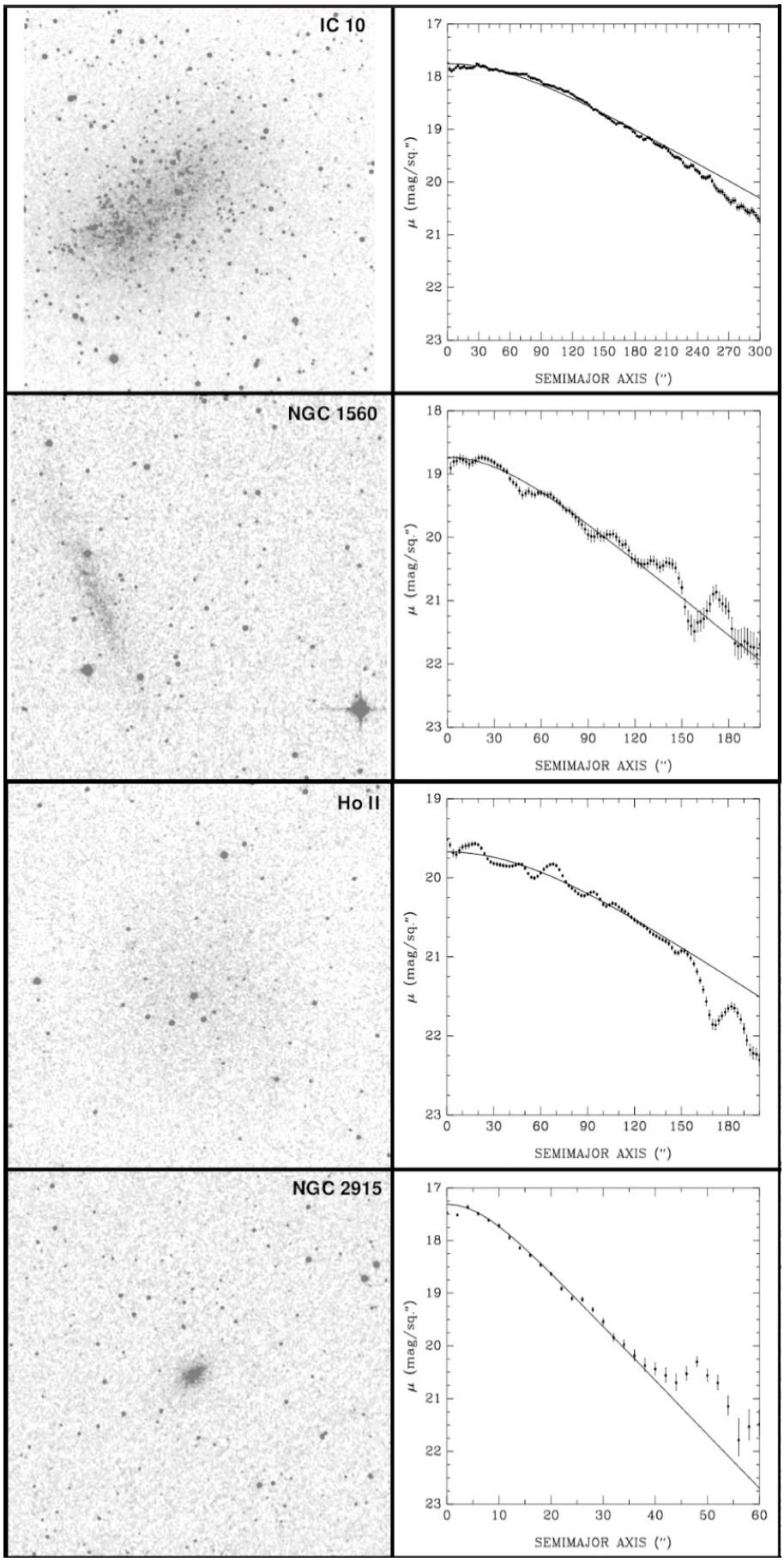

Fig. 1. Images and surface photometry of dIs observed by 2MASS. *Left panels*: K_s images (North is up, East to the left; field of view 8′.5×8′.5). *Right panels*: surface brightness profiles in K_s for the unresolved component. The solid curves are fits of a sech law. In a few instances, a Gaussian burst was fitted simultaneously, and is marked by a dashed curve.

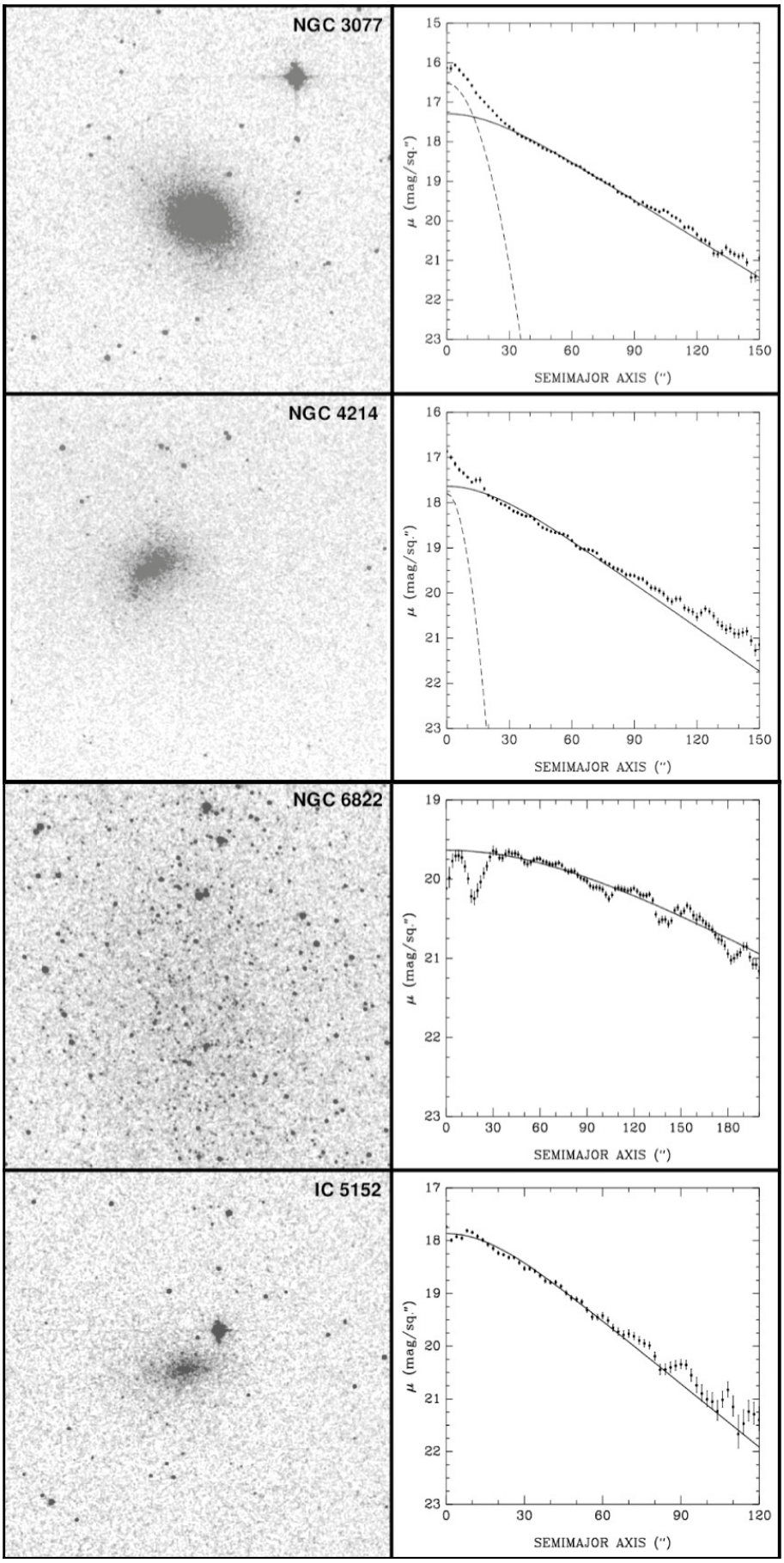

Fig. 1. continued.

Table 1. The observing log for our CFHT 2004 and CTIO 2007 observations.

Galaxy	α (J2000)	δ (J2000)	Observatory	Date (UT)	Exp. time (s)
UGC 3860	07:28:17.4	+40:46:11	CFHT	Feb. 24, 2004	600
UGC 5272	09:50:22.4	+31:29:16	CFHT	Mar. 8, 2004	600
UGC 5340	09:56:45.7	+28:49:35	CFHT	Mar. 8, 2004	600
UGC 5764	10:36:43.3	+31:32:48	CFHT	Mar. 8, 2004	600
UGC 7408	12:21:15.0	+45:48:41	CFHT	Mar. 8, 2004	600
UGC 7490	12:24:25.3	+70:20:01	CFHT	Mar. 8, 2004	600
NGC 4523	12:33:48.0	+15:10:05	CFHT	Mar. 7, 2004	600
UGCA 319	13:02:14.4	–17:14:15	CFHT	Mar. 7, 2004	600
WLM N & S	00:01:58.1	–15:27:39	CTIO	Aug. 3, 2007	1200 and 540
ESO 349-031	00:08:13.3	–34:34:42	CTIO	Aug. 3, 2007	1260
ESO 245-005	01:45:03.7	–43:35:53	CTIO	Aug. 3, 2007	660
ESO 320-14	11:37:53.2	–39:13:13	CTIO	Aug. 3, 2007	1320
ESO 321-014	12:13:49.6	–38:13:53	CTIO	Aug. 3, 2007	1200
KK98 200	13:24:36.2	–30:58:19	CTIO	Aug. 3, 2007	1200
ESO 325-11	13:45:00.5	–41:51:40	CTIO	Aug. 3, 2007	1260
ESO 223-09	15:01:08.7	–48:17:26	CTIO	Aug. 3, 2007	960

second was clear, the sky being bright (two days from Full Moon). Data were reduced, calibrated, and analysed in the same manner as described above for CFHT. Typically, 10 to 15 2MASS stars were employed to calibrate each field.

Imaging and photometry for nine targets are presented here. In the left panels of Fig. 3, we show the reduced CTIO images, while in the right panel we display the surface photometry and the sech fits. In the third section of Table 2, we give the fitting parameters and magnitudes.

6. Homogenized distances

Most distances adopted in this paper are based upon either Cepheid variables or the TRGB. For some galaxies, it has been necessary to use the brightest blue stars or the Hubble law to derive distances.

Following V05, all distances have been homogenized to a common distance scale anchored to the maser distance of NGC 4258 (Herrnstein et al. 1999). Additionally, care was taken to correct all distance indices for extinction using an algorithm which appropriately accommodates effective wavelength shifts (McCall 2004). HST Key Project distances to Cepheid calibrators were appropriately revised (see Fingerhut et al. 2007), and those for which the TRGB was observed were used to calibrate absolute magnitudes. In the I band, the TRGB has been found to be nearly invariant over a wide range of metallicities, thereby serving as a powerful standard candle. Our calibration yields $M_{I,\mathrm{TRGB}} = -3.881 \pm .05$ mag (on the maser zero-point). Fifteen new dwarfs presented in this paper have distances determined from the tip of the red giant branch.

To calculate Hubble distances (for most CFHT targets), we employed velocities listed in NED[1] in the Virgo and Great Attractor flow model (following Mould et al. 2000). Given the choice of the maser zero-point, we adopted $H_0 = 80\,\mathrm{km\,s^{-1}\,Mpc^{-1}}$ (Fingerhut et al. 2007).

All Galactic extinctions presented in Table 2 (τ_1) originate from reddenings of Schlegel et al. (1998), $E(B-V)$, calculated by NED. The reddenings were converted to broadband extinctions using the York Extinction Solver (YES), the foundations of which are described by McCall (2004)[2].

[1] NASA/IPAC Extragalactic Database, http://nedwww.ipac.caltech.edu/ accessed on Jan. 25, 2008.

[2] The York Extinction Solver (YES) is a web-based application developed in the Department of Physics and Astronomy, York University and hosted by the Canadian Astronomy Data Centre (CADC). It can be accessed at http://cadcwww.hia.nrc.ca/yes

Given the reddening for a target, YES computes the corresponding optical depth at 1 μ (τ_1) using the spectral energy distribution for an elliptical galaxy (the type of galaxy to which the reddenings of Schlegel et al. (1998). YES then converts this value for a particular target into broadband extinctions in desired filters using an appropriately redshifted and extinguished spectral energy distribution for the target (in our case, Im). By employing YES to calculate broadband extinctions, we avoid source-dependent shifts in the effective wavelengths of broadband filters.

7. The fundamental plane

In a previous paper (V05), we discovered the "fundamental plane" (FP) of dwarf irregular galaxies (dIs) using photometric data for 19 objects observed in the field and having radio data from the literature. Most targets were selected to have accurate distances derived from Cepheids and the TRGB. We defined the plane in K_s, expressing the absolute sech magnitude (M_{KS}) derived from the sech model (i.e., m_{SK}) as a function of the central surface brightness for the sech model (μ_{0K}) and the 20% width of the HI line profile (W_{20}).

In this paper, we augment our study of the FP by adding the 25 new dwarfs presented in Sects. 4 and 5, which increases the size of our sample to 44 objects. From this sample, we select 34 dIs to refine the FP equation.

For most brighter dwarfs (V05 and CFHT samples), we employ line widths W_{20} from the RC3 catalog (de Vaucouleurs 1991), while for fainter targets (CTIO 2007 sample) we take W_{20} from Huchtmeier et al. (2000, 2001) and HIPASS (Koribalski et al. 2004). In four cases (ESO 320-14, ESO 321-14, ESO 325-11, and ESO 349-31) no W_{20} is available, so we calculate W_{20} using the scaling factor $W_{20}/W_{50} = 1.45$, taking W_{50} from Karachentsev et al. (2004).

In Fig. 4, we plot the Tully-Fisher relation for all dwarfs presented in this paper. This figure definitively shows that the TF relation breaks down for dwarf galaxies. In Fig. 5, we plot the dwarf fundamental plane, coefficients for which have been defined by the 34 dIs for which data are most reliable (see below). The galaxies from V05 are marked by filled circles. 2MASS galaxies are shown as filled triangles, CFHT 2004 galaxies by

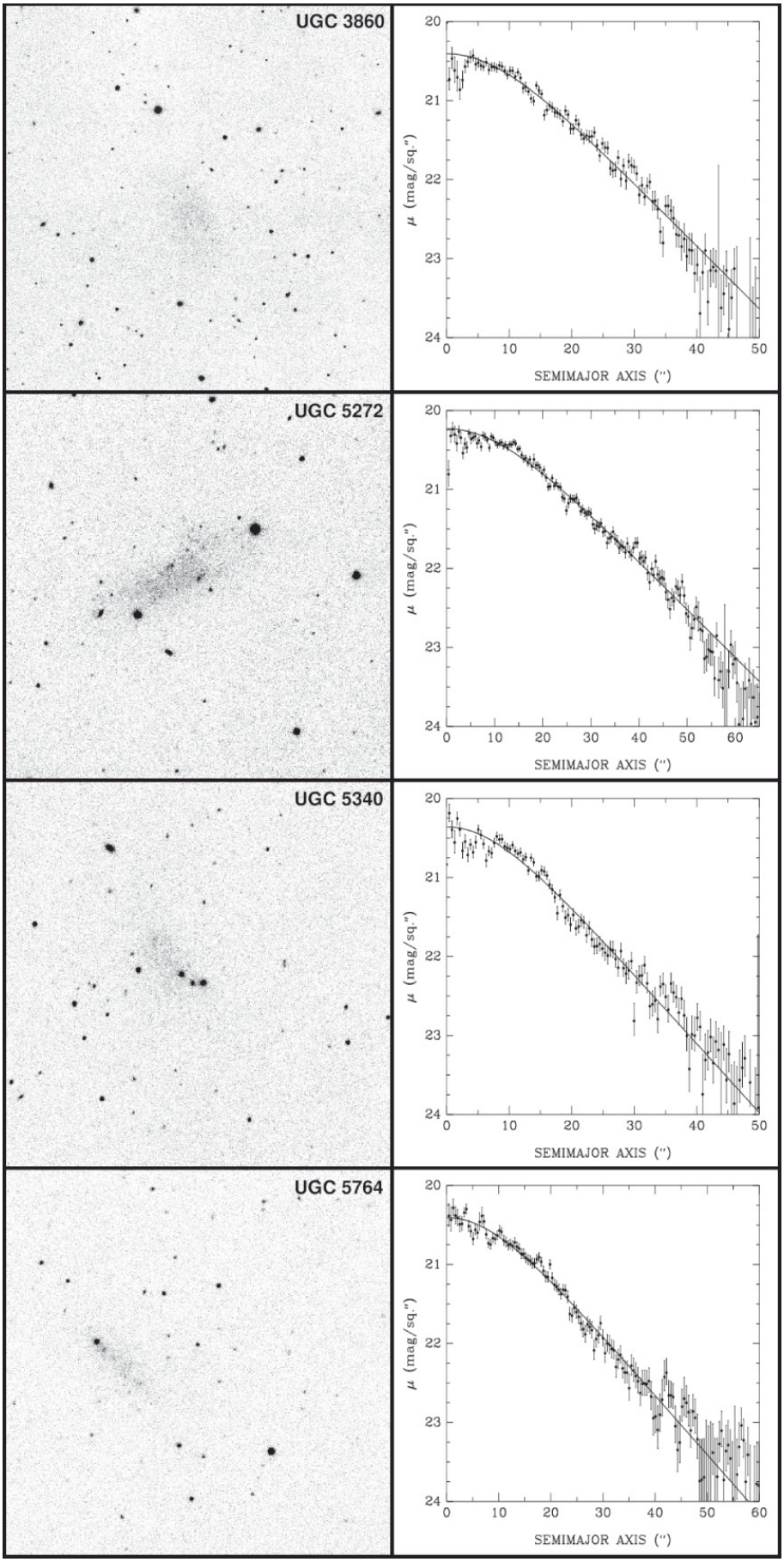

Fig. 2. Images and surface photometry of dIs observed at CFHT. *Left panels*: K_s images (North is up, East to the left; field of view $3\farcm2 \times 3\farcm2$). *Right panels*: surface brightness profiles in K_s for the unresolved component. The solid curves are fits of a sech law. In a few instances, a Gaussian burst was fitted simultaneously, and is marked by a dashed curve.

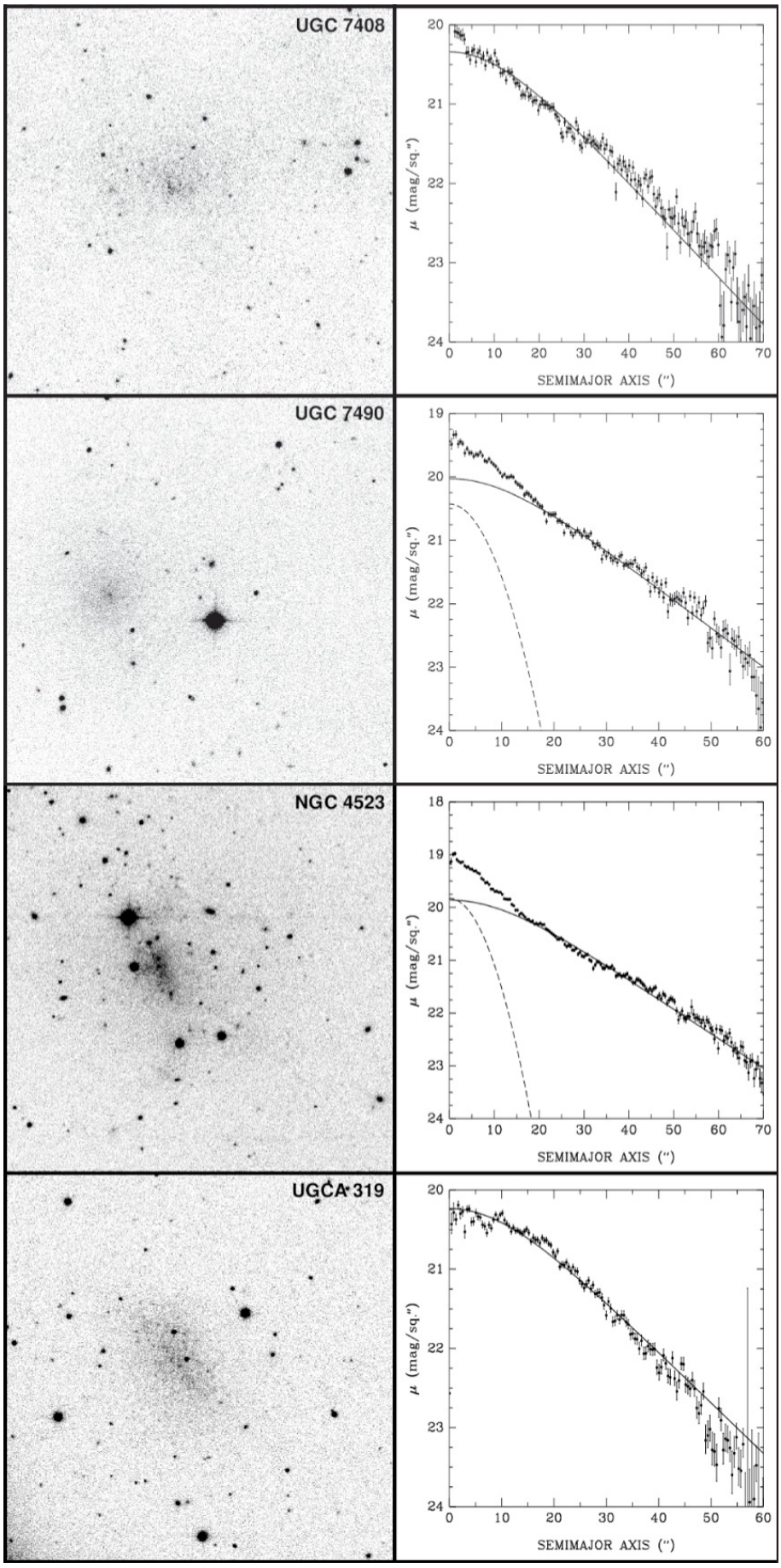

Fig. 2. continued.

Table 2. Photometric parameters for the 2MASS sample (first group), CFHT 2004 sample (second group), and CTIO 2007 sample (third group).

Galaxy[a]	μ_{0K}[b]	r_{0K}[c]	m_{SK}[d]	m_{TK}[e]	PA[f]	e[g]	W_{20}[h]	τ_1[i]	A_{KS}[j]	DM[k]	Method[l]	Ref.[m]
IC 10	17.75	97.8	6.13	6.51	–55	0.6	85	1.78	0.56	24.10	CEPH	F00
NGC 1560	18.73	54.9	9.13	9.26	+23	0.8	157	0.21	0.07	27.56	TRGB	K03a
Holmberg II	19.67	84.3	7.45	8.00	+20	0.0	72	0.04	0.01	27.48	TRGB	K02a
NGC 2915	17.32	10.6	9.93	9.70	–50	0.3	153	0.31	0.10	27.76	TRGB	K03b
NGC 3077	17.30	33.3	7.42	7.32	+40	0.3	91	0.08	0.02	27.75	TRGB	S01
NGC 4214	17.64	33.6	8.11	8.14	–55	0.5	86	0.03	0.01	27.31	TRGB	M02
NGC 6822	19.64	106.8	7.08	7.30	+10	0.2	75	0.27	0.09	23.50	CEPH	V00
IC 5152	17.87	27.1	9.04	9.13	–70	0.6	100	0.03	0.01	26.41	TRGB	K02b
UGC 3860	20.41	13.6	12.83	13.07	+30	0.5	51	0.07	0.02	28.85	HUB	H03
UGC 5272	20.24	17.9	12.31	12.45	–65	0.6	108	0.02	0.01	29.15	HUB	G04
UGC 5340	20.36	12.4	12.79	12.82	+30	0.4	97	0.02	0.01	29.00	HUB	RC3
UGC 5764	20.41	14.5	13.26	13.41	+50	0.7	120	0.02	0.01	29.36	HUB	RC3
UGC 7408	20.34	18.1	11.95	12.03	–75	0.4	51	0.01	0.00	29.29	HUB	RC3
UGC 7490	20.03	17.5	11.91	11.33	+20	0.5	73	0.03	0.01	30.01	HUB	UZC
NGC 4523	19.86	19.3	11.34	11.41	+30	0.4	144	0.04	0.01	29.03	3BS	T00
UGCA 319	20.23	16.9	11.99	12.21	+30	0.4	108	0.09	0.03	29.11	HUB	K04
WLM	21.30	98.1	9.68	9.91	+10	0.6	74	0.04	0.01	24.74	TRGB	M98
ESO 349-031	21.21	12.3	13.34	13.28	0	0.2	29	0.01	0.00	27.36	TRGB	K06
ESO 245-005	20.74	54.6	10.15	10.26	–60	0.5	85	0.02	0.01	28.07	TRGB	K03c
ESO 320-14	20.28	10.9	13.00	12.90	+90	0.4	29	0.16	0.05	28.78	TRGB	K07
ESO 321-014	21.22	23.0	12.13	12.52	+20	0.3	36	0.11	0.03	27.35	TRGB	K05
KK98 200	20.53	8.7	13.55	13.42	–75	0.3	34	0.08	0.02	28.08	TRGB	K05
ESO 325-11	21.43	32.8	11.75	12.20	–50	0.4	96	0.10	0.03	27.50	TRGB	K05
ESO 223-09	19.30	34.5	9.34	9.44	–50	0.3	89	0.30	0.10	28.92	TRGB	K07
ESO 461-036	20.62	13.1	13.13	13.30	+20	0.5	71	0.34	0.11	29.34	TRGB	K06

[a] Galaxy Name. [b] Central surface brightness (from sech law) in mag/arcsec^2. [c] Scale length (from sech law) in arcsec. [d] Apparent sech magnitude (from sech law) in mag. [e] Apparent isophotal magnitude in mag. [f] Position angle (from N to E) in deg. [g] Ellipticity (measured with the STSDAS/ELLIPSE task as a fixed parameter according to V05). [h] Width of the HI line profile measured in km s^{-1} at 20% of the peak. [i] Optical depth at 1 μ (τ_1) calculated by YES. [j] Extinction in K_s band in mag. [k] Distance modulus. [l] Method for distance determination: CEPH – Cepheids, TRGB – Tip of the RGB, HUB – Hubble flow, 3BS – Brightest 3 blue stars. [m] Reference for distance determination (please see References section).

crosses, and the CTIO 2007 galaxies by empty circles. Symbols for the objects with the most accurate distances (TRGB, CEPH) are encompassed by squares.

Of the 25 new objects, 10 deviate by more than 2σ (about 1 mag) with respect to the 34 galaxies defining the FP. NGC 3077 and Holmberg II (from the 2MASS sample) have accurate distances, but they are known to have tidal interactions in the M 81–M 82–NGC 3077 system (e.g., Walter et al. 2006). UGC 7408 and UGC 7490 (from the CFHT sample) are the most distant dwarfs observed, being 8 and 9.2 Mpc away, respectively (Hunter & Elmegreen 2004). Distances had to be derived from the Hubble law. Moreover, both galaxies appear to have light profiles which look more exponential than sech, UGC 7490 being listed by NED as a spiral (SAb). Notably, too, very few 2MASS stars were available to calibrate the UGC 7408 data. Profiles of ESO 223-09 and ESO 245-05 (from the CTIO sample) also appear exponential in shape. At the bright end of the luminosity scale, NGC 2915 and NGC 4214 (from the 2MASS sample) have accurate distances, but they appear deviant, possibly reflecting the limitations of 2MASS photometry. At the faint end, the deviants are ESO 320-14 and ESO 321-014 (from the CTIO sample). Deeper imaging will be necessary to pinpoint why.

We derived the FP using the "best" 34 dIs (19 from the first sample, plus 15 new objects with deviations less than 2σ). These 34 are what remained after iteratively rejecting the most extreme deviants until a point was reached where further rejections had little impact on the fit. The improved equation of the FP is:

$$M_{SK} = (-3.98 \pm 0.42)\log(W_{20}) + (0.70 \pm 0.07)\mu_{0K} - (22.83 \pm 1.85). \quad (2)$$

The fit has a rms deviation of 0.43 mag and a correlation coefficient 0.90. Although it could not decrease the rms in comparison with our previous fit in V05, we were able to reduce the errors of the coefficients by about 30%.

Uncertainties in central surface brightnesses are dominated by calibration errors. Typically, we estimate the uncertainties to be under 0.1 mag. Uncertainties in the line widths are typically 10%. As can be seen from Eq. (2), the line width errors dominate uncertainties in the abscissae of Fig. 5. We estimate a typical error of 0.2 mag in total, which is displayed in the upper left corner of Fig. 5. Uncertainties in the absolute magnitudes are dominated by errors in distances. For the TRGB method, the average uncertainties amount to about 0.18 mag. HUB distances are uncertain by at least 12% based upon the uncertainty in the Hubble constant (V05), but of course actual uncertainties must be considered to be higher for such nearby objects due to peculiar motions. Apparent sech magnitudes are coupled to central surface brightnesses, so their uncertainties are typically around 0.1 mag. Overall, we estimate that uncertainty in M_{KS} is typically 0.2 mag, which is displayed in the upper left corner of Fig. 5.

Considering the uncertainties in both abscissae and ordinates, it is reasonable to expect observational errors to lead to vertical scatter about the fundamental plane amounting to about 0.3 mag. This is less than the observed rms of 0.43 mag, indicating that there remain unexplained contributions to the noise.

To explore whether varying inclinations might be a source of scatter, we examined how the FP changes when line widths or central surface brightnesses are corrected for tilt. First, we estimated the inclination i for each galaxy from the ellipticity listed in Table 2 using the prescription of Staveley-Smith et al. (1992)

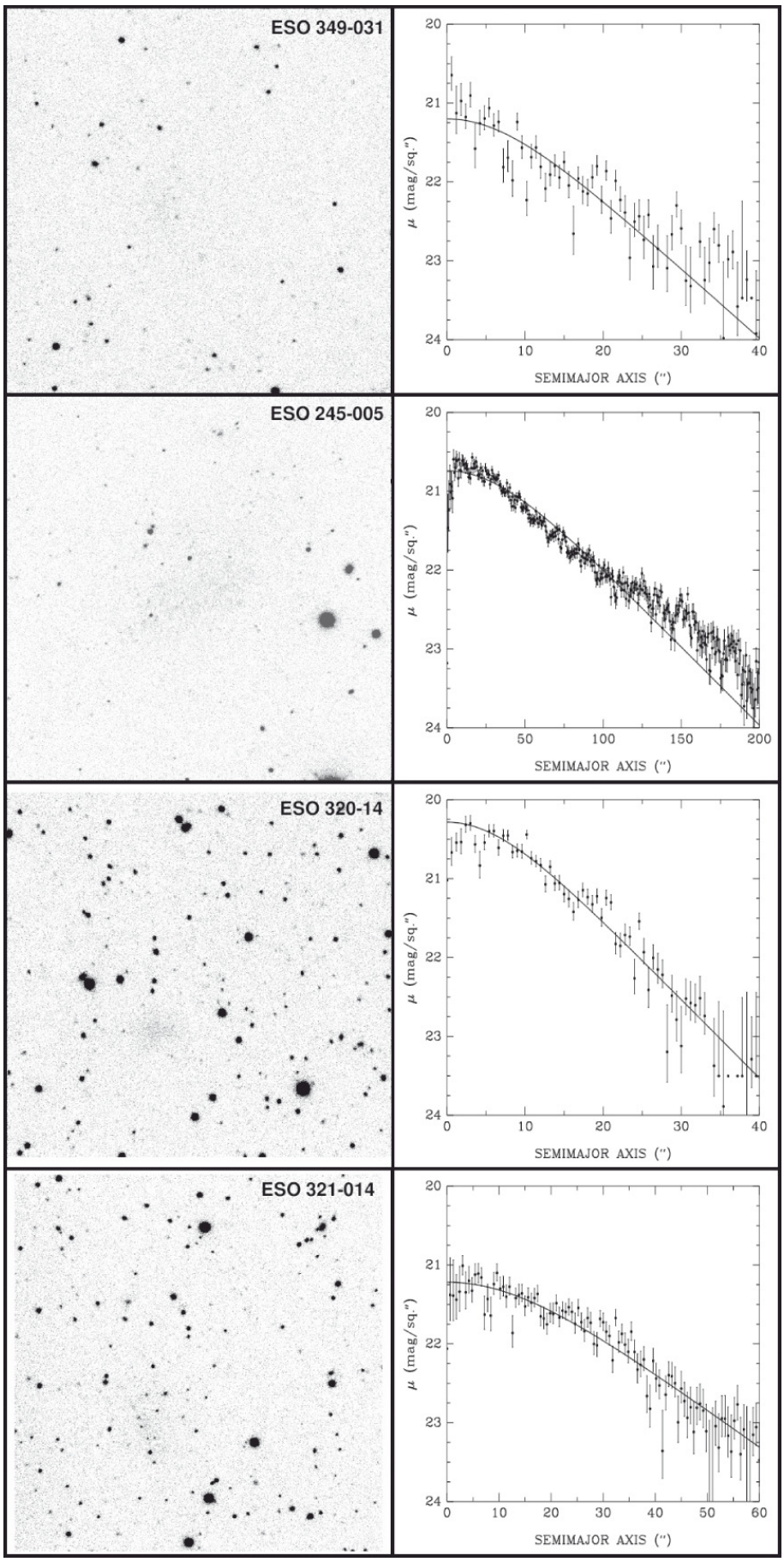

Fig. 3. Images and surface photometry of dIs observed at CTIO. *Left panels*: K_s images (North is up, East to the left; field of view $10\farcm2 \times 10\farcm2$). *Right panels*: surface brightness profiles in K_s for the unresolved component. The solid curves are fits of a sech law.

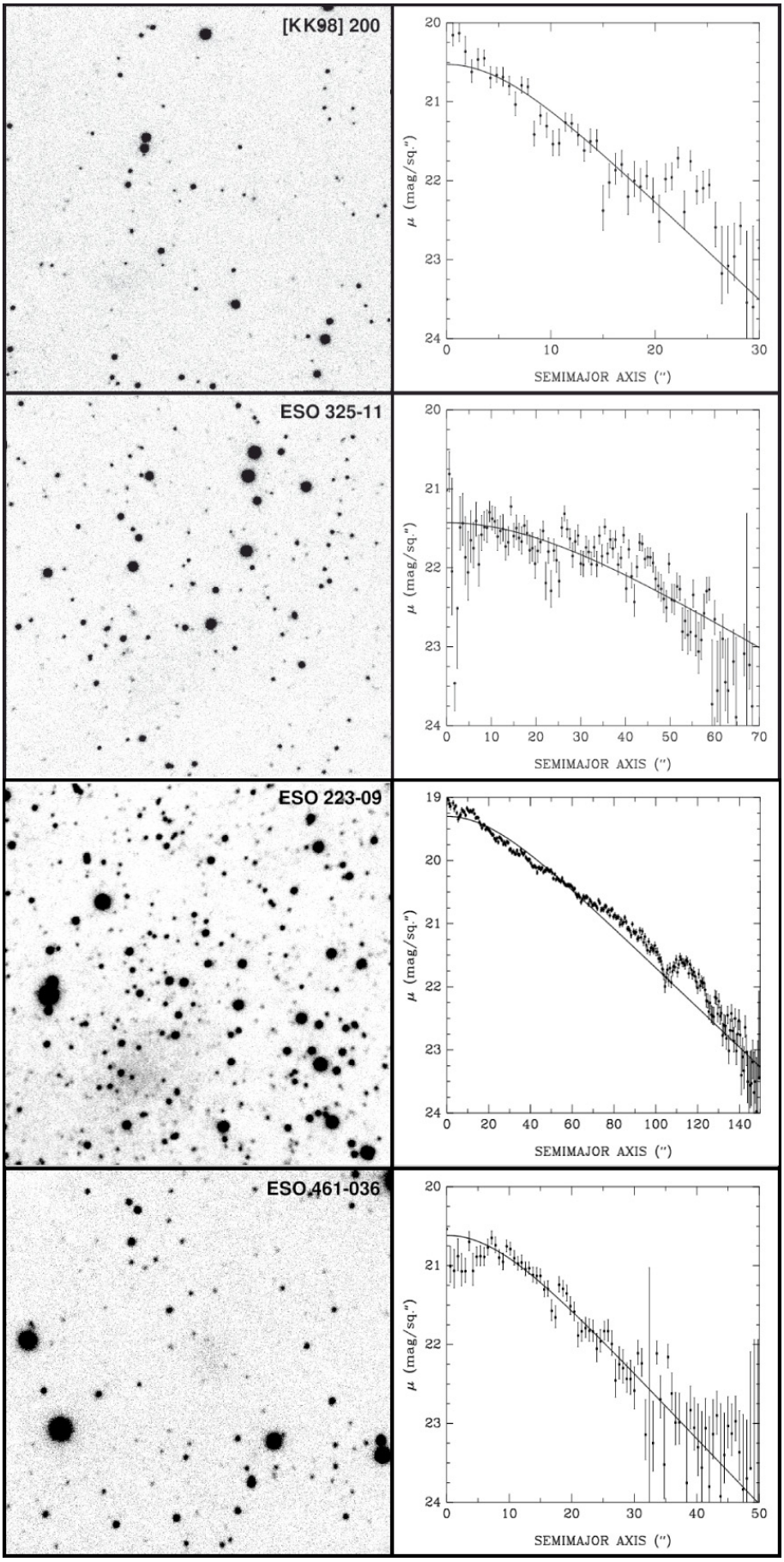

Fig. 3. continued.

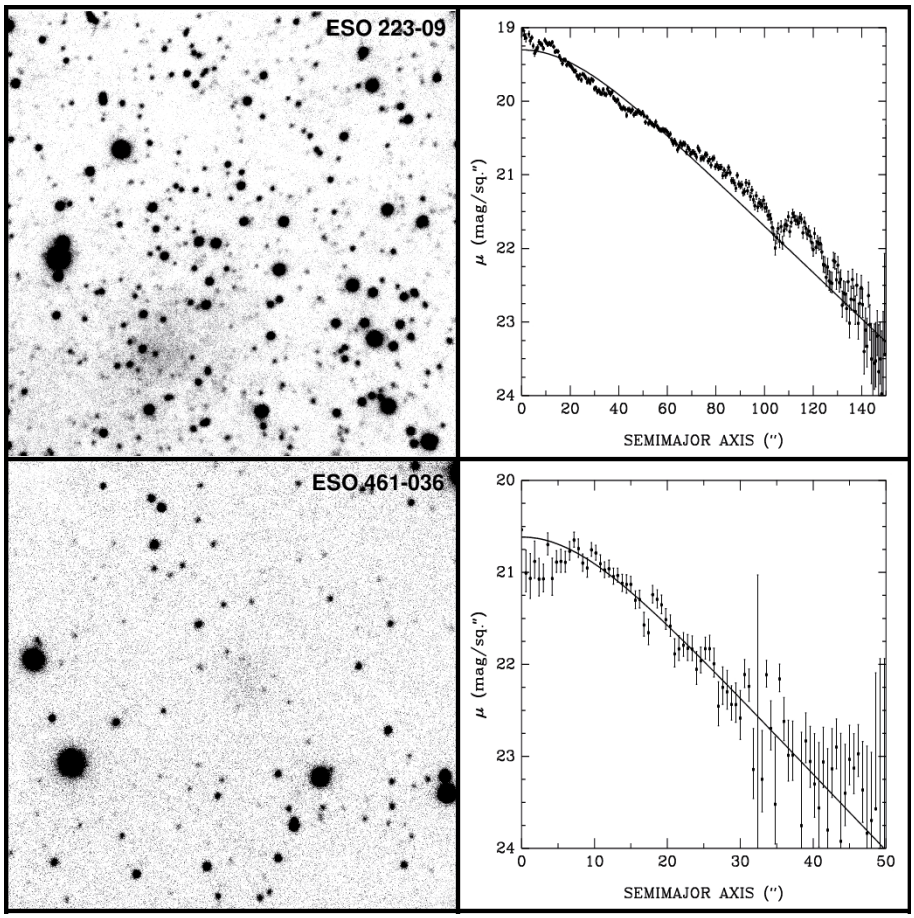

Fig. 3. continued.

for dwarfs. Then, we made the assumption that motions are predominantly rotational, and estimated the rotational velocity from $W_{20}/(2 \sin i)$. Using $W_{20}/(2 \sin i)$ instead of W_{20} as the gauge of kinematics did not yield any improvement to the fit to the FP. The result indicates that internal motions in the majority of the dwarfs are predominantly random. This is a major advantage of the dI FP over the TF relation for spirals, in the sense that distances can be determined without correcting W_{20} for tilt.

How μ_{0K} is corrected for tilt requires an assumption about the intrinsic shape of the galaxies. Both prolate and oblate geometries were considered. We computed the surface brightness at the orientation yielding circular isophotes from $\mu_{0K,\mathrm{face-on}} = \mu_{0K} \pm 2.5 \log(b/a)$, with the plus applicable to the prolate case and the minus to the oblate. Neither approach to correcting surface brightnesses led to any improvement in the fit to the FP.

In summary, using an enlarged sample of galaxies, we have confirmed the existence of the dI FP. However, there remains scatter which is unexplained by formal observational errors, although some of it is likely due to photometry which is too shallow. Also, a few galaxies appear to be distorted by tidal interactions and a few may be massive enough that rotational motions predominate over random ones (in which case, deviance can arise from not correcting the line width for tilt). With the aid of additional data, we plan to examine outliers in more detail in a future paper.

8. Other dwarfs and the dI FP

The dI FP provides a baseline with which to assess linkages with other kinds of dwarfs, such as Blue Compact Dwarfs (BCDs) and dwarf Ellipticals (dEs). Preliminary work by Vaduvescu (2005) suggested that BCDs and dEs lie close to the dI FP. Here, we examine relationships further using our improved FP determination.

8.1. BCDs on the FP

In a previous paper (Vaduvescu, Richer & McCall 2006) we presented deep NIR data for 16 BCDs located in the Virgo cluster. We showed that surface brightness profiles of BCDs can be fitted accurately (within 0.1 mag) by the sum of two components: a hyperbolic secant (sech) to model the overall profile, and a Gaussian component to trace the starburst near the centre of the galaxy. By comparing parameters of the sech fits, it was shown that BCDs appear to be physically similar to dIs. Also, their chemical properties track those of dIs (Vaduvescu et al. 2007).

To place our BCDs on the dI FP, we adopt a distance modulus of 30.62 for the Virgo Cluster (Freedman et al. 2001), which is the HST Key Project value but anchored to the maser distance for NGC 4258. For magnitudes and surface brightnesses, we adopt those of the sech component.

Figure 6 includes 16 BCDs from Virgo and 3 BCDs in the field plotted with respect to the FP defined by Eq. (2) (represented by the dotted line). BCDs are plotted as triangles. Most BCDs lie close to the FP.

8.2. dEs on the FP

Unlike dIs and BCDs, dwarf elliptical galaxies (dEs) and dwarf spheroidals (dSphs) are known to harbour old stellar populations with no traces of gas or star forming regions. A linkage between dIs and dEs was signaled originally through pair-wise

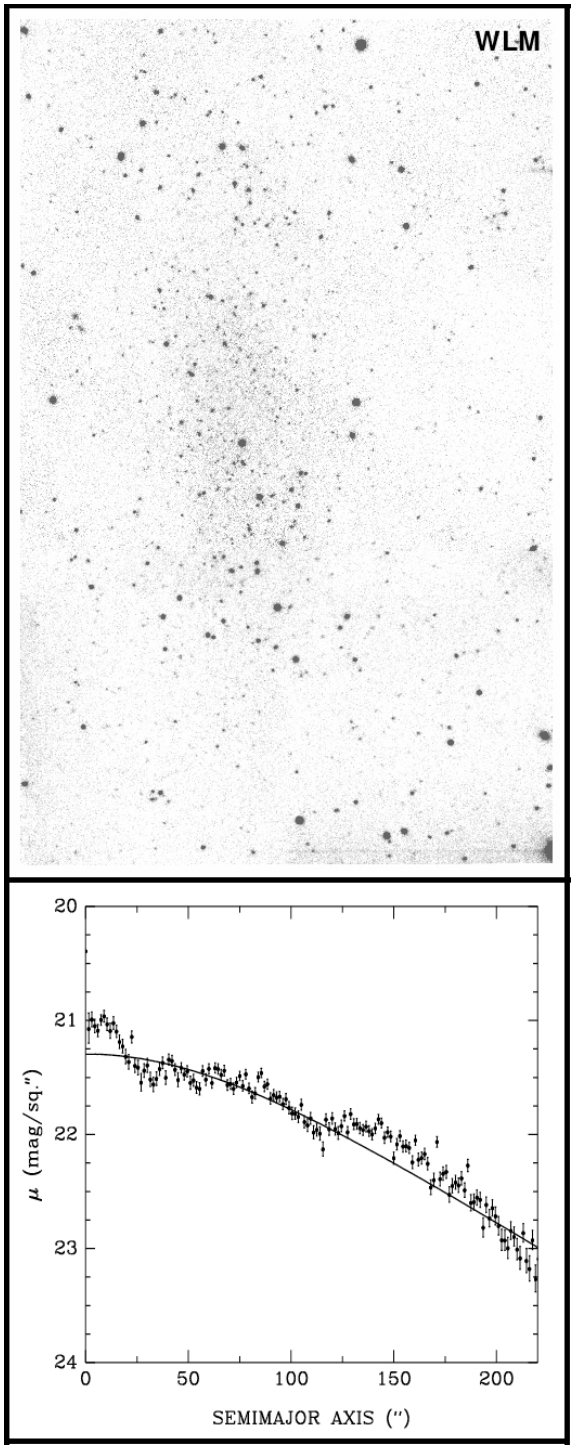

Fig. 3. continued. *Top panel*: WLM image mosaiked from North and South frames (North is up, East to the left; field of view 10′.2 × 16′.1). *Bottom panel*: surface brightness profile in K_s of the unresolved component, with the fitted sech function shown as a solid curve.

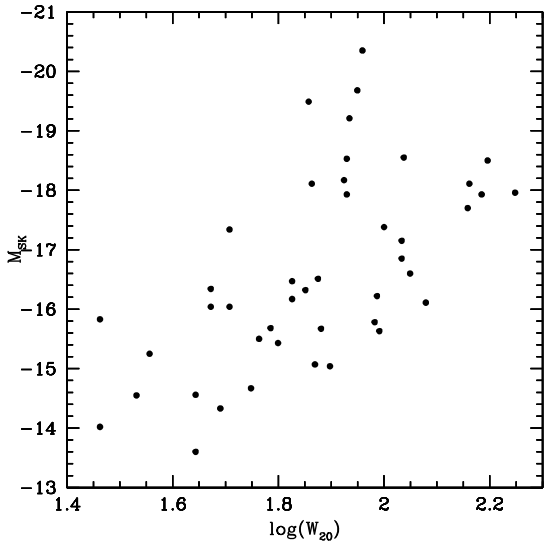

Fig. 4. The Tully-Fisher relation for dIs. No corrections for inclination have been applied. The vertical scale is the same as for the fundamental plane plotted in the next figure.

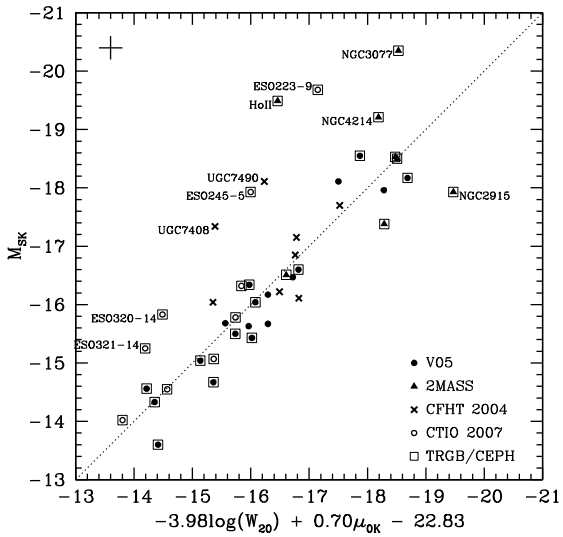

Fig. 5. The fundamental plane for dIs. No corrections for inclination have been applied. Different symbols are used to distinguish the different sources of observations. Objects with accurate distances (TRGB, CEPH) are emphasized with squares. Ten labeled objects lie off the plane (deviating by more than 2σ). Errors in distance are unlikely to be responsible. Rather, many of these objects probably need deeper photometry, although a few may be mis-classified as dwarfs, and a few may be affected by proximity to a massive neighbour (see Sect. 7). The dotted line represents the FP re-defined in this paper using 34 objects (Eq. (2)). Typical uncertainties in abscissae and ordinates are depicted by the error cross in the upper left corner.

comparisons of structural and kinematic parameters (Kormendy 1985). Also, dEs and dIs proved to be more closely related than dEs and giant ellipticals . However, Papaderos et al. (1996) did not find a clear evolutionary connection between dEs, dIs, and BCDs.

The dI FP offers a more refined avenue for exploring how dIs and dEs may be related. A first attempt was presented by Vaduvescu & McCall (2005) and Vaduvescu (2005) who employed 22 dEs located in the Virgo Cluster and the Local Group. The same sample is used here. Data were selected as follows:

– 1. 11 dEs in the Virgo Cluster, with *H* band images from the GOLDMine database (Gavazzi et al. 2002) and velocity dispersions from Geha et al. (2003);
– 2. 3 dEs/dSphs in the Local Group (M 110, NGC 147, NGC 185), with K_s images from the 2MASS Large Galaxies

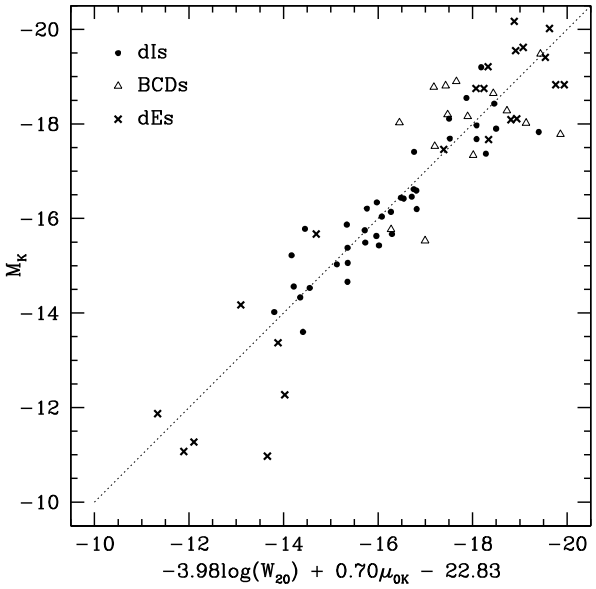

Fig. 6. dIs, BCDs, and dEs on the dI fundamental plane. dIs were fitted using a sech law, BCDs using a sech plus Gaussian, and dEs using an exponential. BCDs and dEs lie on the FP defined by the dIs, suggesting deep physical connections between the three dwarf classes.

Atlas (Jarett et al. 2003) and velocity dispersions from McElroy (1995) and Held et al. (1992);

– 3. 8 dSphs orbiting our Galaxy (Carina, Draco, Fornax, Leo I, Leo II, Sculptor, Sextans, Ursa Minor) for which we could define surface brightness profiles based on star counts in V (Irwin & Hatzidimitriou 1995).

As before, absolute magnitudes for Virgo objects were calculated using a distance modulus of 30.62. For the dEs/dSphs lacking K_s data, we derived magnitudes and surface brightnesses in K_s by adopting mean colours of $H - K_s = 0.2$ (with a scatter of about 0.05 mag) and $V - K_s = 2.7$ mag (with a scatter of about 0.3 mag). These offsets were determined by computing the averages for 22 dEs with K, H and V magnitudes from GOLDMine (Gavazzi et al. 2002). To transform stellar velocity dispersions σ to velocity line widths W_{20}, we used $W_{20} = 3.588\sigma$ as derived from a standard normal distribution model of the stellar velocity dispersions.

Surface brightness profiles of dEs are peaked at small radii (i.e., a convex function), so cannot be modeled by a sech function. Combining a sech function with a Gaussian, as we did for BCDs, also does not work because of the sharpness of the cores. Instead, we adopted an exponential model to fit surface brightness profiles of dEs. An exponential was shown to fit profiles of dEs by Kormendy (1977), Faber & Lin (1983) and Binggeli et al. (1984). The exponential law has two parameters, the central surface brightness and the scale length, i.e., the same degrees of freedom as the sech law for dIs and BCDs. To fit the profiles, we restricted the exponential to the linear part of the fit, preventing the core which in most cases was a small fraction from the entire profile (around 10%). The absolute magnitude was computed from the apparent magnitude of the exponential model.

Figure 6 shows the dEs plotted with respect to the FP defined by Eq. (2) (the dashed line). Despite the approximations made to extract photometric parameters, the dEs fall on the FP defined by the dIs over a 9 mag interval in absolute magnitude.

9. Conclusions

New NIR photometry for dIs has been presented, leading to an expanded sample of 44 galaxies with which to study the fundamental plane discovered by Vaduvescu et al. (2005). As before, it has been appropriate to define photometric parameters by fitting a sech function to the surface brightness profiles. The FP remains clearly defined, with the rms K_s absolute magnitudes for the 34 galaxies used in the fit being 0.43 mag (as in the original paper). Correcting line widths for inclination did not lead to any reduction in the rms, indicating that internal motions are predominantly random. Correction of surface brightnesses for tilt led to no improvement, too, regardless as to whether geometries were assumed to be prolate or oblate. The results suggest that the FP can be used to derive dwarf distances without knowing tilts.

The new fit to the dI FP has been used to evaluate linkages to BCDs and dEs. Light profiles of BCDs were fit as a combination of a Gaussian burst on top of an underlying distribution defined by a sech function. Adopted photometric parameters were derived from the shape of the sech function. With photometric parameters defined this way, BCDs fall precisely on the FP defined by dIs. dEs light profiles cannot be modeled using a sech function. Instead, we fitted their overall envelopes with an exponential, and used the parameters ot the exponential to define photometric parameters for the FP. When parametrized this way, dEs also lie on the FP defined by dIs. The outstanding overlap of the three dwarf classes suggests strong linkages among dIs, BCDs, and dEs. The simplicity of light profiles and chemistry of dIs motivates using them as a control for the evolutionary studies of other dwarf galaxies.

Acknowledgements. This publication makes use of data products from the Two Micron All Sky Survey (2MASS), which is a joint project of the University of Massachusetts and the Infrared Processing and Analysis Center/California Institute of Technology, funded by the National Aeronautics and Space Administration and the National Science Foundation. The paper included data based on observations obtained at the Canada-France-Hawaii Telescope (CFHT) which is operated by the National Research Council of Canada, the Institut National des Sciences de l'Univers of the Centre National de la Recherche Scientifique of France, and the University of Hawaii. We acquired some data at Cerro Tololo Inter-American Observatory (CTIO), which is operated by the Association of Universities for Research in Astronomy (AURA), Inc. under a cooperative agreement with the National Science Foundation. This research has made use of the NASA/IPAC Extragalactic Database (NED) which is operated by the Jet Propulsion Laboratory, California Institute of Technology, under contract with the National Aeronautics and Space Administration. This research has made use of the GOLDMine Database (Gavazzi et al. 2002). For our data reductions, we used IRAF, distributed by the National Optical Astronomy Observatories, which are operated by the Association of Universities for Research in Astronomy, Inc., under cooperative agreement with the National Science Foundation. M.L.M. thanks the Natural Sciences and Engineering Council of Canada for its continuing support. Special thanks are due to the anonymous referee who provided valuable feedback which allowed us to improve the paper.

References

Bettoni, D., Falomo, R., Fasano, G., Govoni, F., et al. 2003, New A Rev., 47, 179
Binggeli, B., Sandaga, A., & Tarenghi, M. 1984, AJ, 89, 64
Buta, R., & McCall, M. L. 1999, ApJS, 124, 33
Cote, S., Freeman, K. C., Carignan, C. Q., & Peter, J. 1997, AJ, 114, 1313 (C97)
de Vaucouleurs G., et al. 1991, Third Reference Catalog of Bright Galaxies (New York: Springer) (RC3)
Djorgovski, S., & Davis, M. 1987, ApJ, 313, 59
Faber, S. M., & Jackson, R. E. 1976, ApJ, 204, 668
Faber, S. M., & Lin, D. N. C. 1984, ApJ, 266, L17
Falco, E. E., Kurtz, M. J., Geller, M. J., et al. 1999, PASP, 111, 438, The Updated Zwicky Catalog (UZC)
Ferrarese, L., Ford, H. C., Huchra, J., et al. 2000, ApJS, 128, 431 (F00)

Fingerhut, R. L., Lee, H., McCall, M. L., & Richer, M. G. 2007, ApJ, 655, 814
Freedman, W. L., Madore, B. F., Gibson, B. K., et al. 2001, ApJ, 553, 47
Garrido, O., Marcelin, M., & Amram, P. 2004, MNRAS, 349, 225 (G04)
Gavazzi, G., Boselli, A., Donati, A., Franzetti, P., & Scodeggio, M. 2003, A&A, 400, 451
Gavazzi, G., Boselli, A., Cortese, L., et al. 2006, A&A, 446, 839
Geha, M., Guhathakurta, P., & van der Marel, R. P. 2003, AJ, 126, 1794
Hamilton, T. S., Casertano, S., & Turnshek, D. A. 2006, New A, 50, 758
Han, J., Deng, Z., Zou, Z., Wu, X.-B., Jing, Y., et al. 2001, PASJ, 53, 853
Held, E. V., et al. 1992, AJ, 103, 3, 851
Herrnstein, J. R., Moran, J. M., Greenhill, L. J., et al. 1999, Nature, 400, 539
Huchtmeier, W. K., Karachentsev, I. D., & Karachentseva, V. E. 2000, A&AS, 147, 187
Huchtmeier, W. K., Karachentsev, I. D., & Karachentseva, V. E. 2001, A&A, 377, 801
Huchtmeier, W. K., Karachentsev, I. D., & Karachentseva, V. E. 2003, A&A, 401, 483 (H03)
Hunter, D. A., & Elmegreen, B. G. 2004, AJ, 128, 2170 (H04)
Irwin, M., & Hatzidimitriou, D. 1995, MNRAS, 277, 1354
James, P. A., Shane, N. S., Beckman, J. E., et al. 2004, A&A, 414, 23 (J04)
Jarett, T. H., et al. 2003, AJ, 125, 525
Karachentsev, I. D. 2005, AJ, 129, 178 (K05)
Karachentsev, I. D., Dolphin, A. E., Geisler, D., et al. 2002a, A&A, 383, 125 (K02a)
Karachentsev, I. D., Sharina, M. E., Makarov, D. I., et al. 2002b, A&A, 389, 812 (K02b)
Karachentsev, I. D., Sharina, M. E., Dolphin, A. E., & Grebel, E. K. 2003a, A&A, 408, 111 (K03a)
Karachentsev, I. D., Makarov, D. I., Sharina, M. E., et al. 2003b, A&A, 398, 479 (K03b)
Karachentsev, I. D., Grebel, E. K., Sharina, M. E., et al. 2003c, A&A, 404, 93 (K03c)
Karachentsev, I. D., Karachentseva, V. E., Huchtmeier, W. K., & Makarov, D. I. 2004, AJ, 127, 2031
Karachentsev, I. D., Dolphin, A., Tully, R. B., et al. 2006, AJ, 131, 1361 (K06)
Karachentsev, I. D., Tully, R. B., Dolphin, A., et al. 2007, AJ, 133, 504 (K07)
Koribalski, B. S., Staveley-Smith, L., Kilborn, V. A., et al. 2004, AJ, 128, 16 (K04)
Kording, E., Falcke, H., & Corbel, S. 2006, A&A, 456, 439
Kormendy, J. 1977, ApJ, 217, 406
Kormendy, J. 1985, ApJ, 295, 73
Maiz-Apellaniz, J., Cieza, L., & MacKenty, J. W. 2002, AJ, 123, 1307 (M02)
Mateo, M. L. 1998, ARA&A, 36, 435 (M98)
Makarova, L. N., & Karachentsev, I. 1998, A&AS, 133, 181 (M98)
McCall, M. L. 2004, AJ, 128, 2144
Merloni, A. Heinz, S., & di Mateo, T. 2003, MNRAS, 345, 1057
McElroy, D. B. 1995, ApJS, 100, 105
Mould, J. R., Huchra, J. P., Freedman, W. L., et al. 2000, ApJ, 529, 786
Papaderos, P., Loose, H.-H., Fricke, K. J., & Thuan, T. X. 1996, A&A, 314, 59
Pierini, D., & Tuffs, R. J. 1999, A&A, 343, 751
Reda, F. M., Forbes, D. A., & Hau, G. K. T. 2005, MNRAS, 360, 693
Sakai, S., & Madore, B. F. 2001, ApJ, 555, 280 (S01)
Schlegel, D. J., Finkbeiner, D. P., & Davis, M. 1998, ApJ, 500, 525
Skrutskie, M. F., Cutri, R. M., Stiening, R., et al. 2006, AJ, 131, 1163
Staveley-Smith, L., Davies, R. D., & Kinman, T. D. 1992, MNRAS, 258, 334
Tikhonov, N. A., Galazutdinova, O. A., & Drozdovski, I. O. 2000, Astrofizica, 43, 367 (T00)
Tully, R. B., & Fisher, J. R. 1977, A&A, 54, 661
Vaduvescu, O. 2005, infrared Properties of Star Forming Dwarf Galaxies, Ph.D. Thesis, York University, Canada
Vaduvescu, O., & McCall, M. L. 2004, PASP, 116, 640
Vaduvescu, O., & McCall, M. L. 2005, dEs and the dI fundamental plane, Switzerland, ed. H. Jerjen, & B. Binggeli (Cambridge: Cambridge University Press), IAU Coll. Proc., 198, 265
Vaduvescu, O., McCall, M. L., Richer, M. G., & Fingerhut, R. L. 2005, AJ, 130, 1593 (V05)
Vaduvescu, O., Richer, M. G., & McCall, M. L. 2006, AJ, 131, 1318
Vaduvescu, O., McCall, M. L., & Richer, M. G. 2007, AJ, 134, 604
van den Bergh, S. 2000, PASP, 112, 529 (V00)
Walter, F., Martin, C. L., & Ott, J. 2006, AJ, 132, 2289
Wang, R., Wu, X.-B., & Kong, M.-Z. 2006, ApJ, 645, 890
Woo, J.-H., Urry, C. M., Lira, P., et al. 2004, ApJ, 617, 903